JOURNAL OF Applied Polymer SCIENCE

Frequency and Temperature Dependence of Poly(*N*-isopropylacrylamide) Gel Rheology

Avanish S. Parmar,[1] Shannon Hill,[1] Ajay Vidyasagar,[2] Carlos Bello,[2] Ryan Toomey,[2] Martin Muschol[1]

[1]Department of Physics, University of South Florida, Tampa, Florida 33620

[2]Department of Chemical and Biomedical Engineering, University of South Florida, Tampa, Florida 33620

Correspondence to: M. Muschol (E-mail: mmuschol@usf.edu)

ABSTRACT: Poly(*N*-isopropylacrylamide) or *p*-NIPAAM gels undergo a prominent deswelling transition near physiological temperatures. Using passive microrheology, we have investigated the viscoelastic response of *p*-NIPAAM gels over a frequency range not accessible to bulk rheological measurements. Overall, NIPAAM gels moderately shear stiffen with increasing frequency. More intriguingly, sample viscosity rapidly declines with increasing frequency before leveling off near the solvent viscosity. The frequency for this crossover coincides with the emergence of fast gel modes seen in dynamic light scattering (DLS) from the gel. Furthermore, we monitored viscoelastic responses on approach to the deswelling transition. Intrinsic light scattering indicates that experimental conditions are not near the critical point and that the deswelling transition is second order in nature. Nevertheless, the corresponding elastic and viscous moduli of *p*-NIPAAM displayed power-law decreases with temperature. These changes with temperature were independent of probe frequency. Power law exponents, however, are sensitive to details of the sample preparation suggesting that these viscoelastic responses vary with gel structure. Correlating our microrheological measurements with DLS from the gel matrix itself, we find that several of the observed microrheological features are closely related to the intrinsic dynamics of the *p*-NIPAAM gels. In particular, the transition from gel- to solvent dominated dissipation coincides with a transition from fast to slow gel modes. Combining microrheology with intrinsic light scattering, therefore, provides a compelling approach to probe rheological responses and correlate them to the underlying network dynamics. © 2012 Wiley Periodicals, Inc. J. Appl. Polym. Sci. 000: 000–000, 2012

KEYWORDS: poly(*N*-isopropylacrylamide); dynamic light scattering; polystyrene; viscous modulus; elastic modulus; microrheology; deswelling transition

Received 20 June 2011; accepted 24 February 2012; published online
DOI: 10.1002/app.37561

INTRODUCTION

Gel networks comprising lower critical solution temperature (LCST) polymers have found success in technologies that benefit from reversible modulation of pore size, including drug delivery, chromatography, and flow control.[1–4] The gel pore size in LCST networks is regulated by temperature. At temperatures below the demixing, the entropy of mixing dominates and the gels swell thereby favoring large pores. As the demixing temperature is approached, hydrophobic interactions shrink the pore size.

Poly(*N*-isopropylacrylamide) or *p*-NIPAAM was among the first systems for which a prominent deswelling transition of the gel phase was observed near physiological temperatures ($\sim 32^{\circ}$C).[1,2] The demixing behavior is characterized by a rather flat spinodal, i.e., the spinodal temperature is only very weakly dependent on the polymer concentration. Subtle changes in preparation of the gels, nonetheless, affect how a system approaches the spinodal.[1] Crosslinking effectively freezes in spatial heterogeneities in concentration leading to nonergodicity.[3] As a result, the local behavior of the gel may be different from the averaged behavior of macroscopic samples. This becomes primarily relevant near the demixing temperature, where the distribution in pore sizes is especially sensitive to the built-in heterogeneity. Characterizing viscoelastic behavior locally and over a wide range of time scales as the gel approaches, the spinodal temperature is therefore not just important for interpreting bulk mechanical performance but also for characterizing how spatial modulation of gel properties affect local gel responses.

Most rheological techniques rely on bulk measurements that probe gel responses at long relaxation times and averaged over all spatial heterogeneities. Changes to the rheology of *p*-NIPAAM on crossing the LSCT have been investigated both in polymer solutions and crosslinked gels. *p*-NIPAAm gel rheology has been characterized with bulk dynamic and static

mechanical measurements.[5–7] Measurements across the transition in the gel phase are intrinsically difficult, because the volume of the gel changes drastically near the demixing temperature. Shibayama and Tanaka, to circumvent this issue, studied isochore gel samples at low frequencies (8 Hz) and reported elastic-like behavior below the transition temperature and viscoelastic like behavior above the transition temperature. In all cases, though, the gels studied had high-elastic moduli (10^4–10^6 Pa), exceeding the soft gels investigated in this article by several orders of magnitude.

The advent of microrheological techniques has expanded significantly the range of accessible frequencies and length scales that can be probed.[8] In microrheology, micron-sized probe particles are embedded into the gel matrix, and their (actively or thermally) driven motion is measured either directly using video microscopy or determined through indirect optical detection such as interferometry,[9] dynamic light scattering (DLS), or diffusing wave spectroscopy (DWS).[10–12] Each of these approaches monitors the mean-square displacement of the tracer particles as function of time which, in turn, is then related to the viscous damping and elastic restoring forces imposed by the gel matrix onto the tracer dynamics. A more detailed discussion of the method and associated data analysis is provided in the Experimental section below. In video-based particle tracking, individual particle motion is determined that allows the detection of intrinsic local heterogeneities either at the scale of individual tracer particles (single particle microrheology) or over the size of the measurement volume used to average tracer dynamics.[13] Indirect particle tracking typically relies on light scattering to detect tracer particle motion. Among those, diffusing wave spectroscopy or DWS permits measurements at very high probe frequencies and highly turbid samples but provides no local information. DLS represents a compromise by offering much higher time resolution than video-based measurements while retaining detection volumes with submillimeter dimensions.

Herein, we used indirect particle tracking with DLS to study the elastic and viscous moduli of crosslinked *p*-NIPAAM gels at high frequencies (5–100 kHz) and on approach to the spinodal for thermally induced gel collapse. Specifically, we investigated whether high-frequency viscoelastic behavior of soft *p*-NIPAAM gels could readily be extrapolated from their responses in the low-frequency regime. Furthermore, we were interested in characterizing temperature effects on viscoelastic responses of *p*-NIPAAM gels at off-critical concentrations, i.e., at concentrations distinct from the unique critical concentrations of the *p*-NIPAAMs deswelling transition. Finally, we explored whether the viscoelastic responses of *p*-NIPAAM gels, derived from tracer particle dynamics, could be correlated with the intrinsic dynamics of *p*-NIPAAM gels observed with DLS from gels without embedded tracer particles.

EXPERIMENTAL

Chemicals

N-Isopropylacrylamide (NIPAAM), tetramethylethylenediamine (TEMED), ammonium persulfate, and *N*,*N*′-methylenebisacrylamide (BisAAM) were obtained from Sigma-Aldrich and were reagent-grade or better. Calibrated polystyrene beads (nom. diam of 200 nm, 450 nm, or 900 nm) were from Duke Scientific with average sizes and standard deviation determined per manufacturer TEM calibration. Deionized water from a Barnstead E-pure 4-module system (18.2 MΩ cm) was used for preparation of all aqueous samples.

Gel Preparation

p-NIPAAM solutions were prepared at room temperature by dissolving 10 wt % NiPAAM, 0.2 wt % BisAAm, and 0.04 wt % ammonium persulfate in distilled water. These solutions were passed through syringe filters (0.02 μm pore) to remove any undissolved clusters and bubbled with dry nitrogen gas for 5 min. The mixture was diluted up to two times and TEMED (10 μL per 10 mL of solution) was added to catalyze the reaction. Depending on the degree of dilution, gelation was complete in 10 min or 16 h. When diluted by a factor of 2, gelation occurred between 7 and 16 h. When diluted by a factor of 1.5, gelation was completed in 10 to 15 min. For microrheology measurements, typically 0.005 wt % of polystyrene beads was dissolved in the solution before the onset of gelation. For measurements, before and after completion of gelation, the 2× dilution was used. For all other measurements, the 1.5× dilution was used because it yielded more reproducible gel stiffness. The 1.5× dilution was allowed to incubate for 24–48 h before a measurement was taken. At that point no changes in rheological properties with incubation time were observed.

Microrheology Using DLS

The thermally activated motion of the embedded polystyrene beads was monitored with DLS using a Zetasizer Nano S (Malvern Instruments, UK) with a 4 mW He-Ne laser ($\lambda = 633$ nm). Light back scattered at an angle of 173° was collected by an optical fiber coupled to a photon detector. Glass cuvettes containing the gels with embedded beads as probe particles were placed inside the thermostated sample holder of the DLS unit. Samples were allowed to equilibrate to their set temperatures for a minimum of 5 min before any measurements. During temperature scans, samples were typically equilibrated for 30 min before any measurements. At that point, correlation functions collected at subsequent time points showed no discernable differences. The concentration of 0.005 wt % for the 453 nm beads in our experiments was chosen such that the scattering from the beads was at least five to seven times stronger than from the gel alone. Bead concentrations for the 200 nm and 900 nm beads were adjusted to reach scattering intensities comparable with those for 450 nm beads. At the same time, the bead concentration was kept low enough to avoid multiple scattering. Using a variable ND filter, count rates during the experiments were adjusted to approx. 3×10^5 count/s. Autocorrelation functions of the scattered light intensity were accumulated for 2 min and data analysis was performed using the average of five measurements at each temperature. Measurements of intrinsic static and dynamic light scattering from the

gels without beads proceeded in the same manner as those for the microrheological measurements described above.

Derivation of Viscous and Elastic Responses from Rracer dynamics

DLS measures the intensity correlation function $g_2(\tau)$ of temporal fluctuations in the scattering intensity. For the case of gel samples with beads, fluctuations in the scattering intensity are dominated by the thermal agitation of the polystyrene particles embedded in the gel matrix. The field correlation function $g_1(\tau)$, used in the subsequent analysis of the scattering data, is related to the experimentally measured and normalized intensity correlation function $g_2(\tau)$ through the Siegert relation[14]

$$g_2(\tau) = 1 + g_1^2(\tau). \tag{1}$$

The mean square displacement (MSD) of the polystyrene beads can be derived from the field autocorrelation $g_1(\tau)$ via[12]

$$g_1(\tau) = \exp\left(\frac{-q^2\langle \mathrm{MSD}(\tau)\rangle}{6}\right) \tag{2}$$

where q is the magnitude of the scattering vector given by

$$q = \left(\frac{4\pi n}{\lambda}\right)\sin\left(\frac{\theta}{2}\right) \tag{3}$$

and λ is the laser wavelength, n is the solution's refractive index, and θ is the in-plane angle at which the scattered light is detected. The experimentally measured intercept β (≤ 1) of $g_1(\tau)$ was normalized to $\beta = 1$ before conversion of the field autocorrelation $g_1(\tau)$ into MSD.

Following the approach of Mason,[15] we use the local slope α of the logarithmic derivative of the MSD

$$\alpha = \frac{d[\ln(\mathrm{MSD})]}{d[\ln(\tau)]} \tag{4}$$

which is related to the complex modulus via the generalized Stokes-Einstein equation[15]

$$|G^*(f)| = \frac{k_B T}{\pi\, a\langle \mathrm{MSD}(f^{-1})\rangle \Gamma(1+\alpha(f))} \tag{5}$$

where a is the radius of the tracer bead, $\langle \mathrm{MSD}(f^{-1})\rangle$ and $\alpha(f)$ are the magnitude of the MSD and the local slope defined in eqs. (2) and (4), respectively, both evaluated at $\tau = f^{-1}$ and Γ is the gamma function. The elastic modulus $G'(f)$ and viscous modulus $G''(f)$ are then given by

$$G'(f) = \lceil G^*(f)\rceil \sin\left(\frac{\pi}{2}\alpha(f)\right) \tag{6a}$$

$$G''(f) = \lceil G^*(f)\rceil \cos\left(\frac{\pi}{2}\alpha(f)\right) \tag{6b}$$

The viscous modulus $G''(f)$ is related to the dynamic viscosity η of the gel via

$$\eta = \frac{G''(f)}{f} \tag{7}$$

Finally, the phase angle δ is defined via the ratio of elastic and viscous moduli, i.e.,

$$\tan(\delta) = \frac{G''(f)}{G'(f)} \tag{8}$$

RESULTS AND DISCUSSION

Microrheology of *p*-NIPAAM Before and After Gelation

We used passive optical microrheology to characterize the rheological properties of *p*-NIPAAM gels over frequencies ranging from 10 to 10^5 kHz. In passive optical microrheology, submicron tracer particles are embedded in the gel matrix and the thermal motion of the beads, detected via DLS, is used to evaluate local ($\sim$ 5 nL or $\sim$ 170 μm^3 measurement volume) viscoelastic responses (for a review, see Ref. 12). For beads undergoing purely Brownian motion in a viscous fluid, the MSD of the beads scales linearly with time. When embedded in a viscoelastic gel matrix, the motion turns subdiffusive instead, i.e., MSD $\propto t^{\alpha}$ with $\alpha < 1$. To confirm this prediction and to test our measurement approach, we measured the MSD of submicron polystyrene beads (diam. 453 $\pm$ 4 nm) from the same *p*-NIPAAM solutions before (<15 min) and after (>18 h) gel formation. Tracer particle concentration was adjusted such that the autocorrelation function of scattered light measured in DLS was dominated by the thermal motion of the strongly scattering tracer particles. This condition can not be satisfied for temperatures above the gel collapse which causes a large increase in scattering intensity. Hence, we limited our measurements to temperatures just up to the deswelling transition, or approximately 33 C [see also Figure 8(a)].

Figure 1(a) displays the correlation function of light scattered from tracer particles in *p*-NIPAAM solution before the onset and well after completion of gelation at 30°C. As indicated by the noticeably slower relaxation rates in the gelled-out phase, correlations in the positions of tracer particles persist significantly longer compared with the corresponding solution sample. MSDs vs. time and the corresponding logarithmic slope α were derived from the correlation data using eqs. (2) and (4) (see Experimental section). In the nascent stages of gelation [Figure 1(b)], the MSD increases linearly with time t, with a constant slope α equal to 1. The drop off in the slope beyond delay times of 10^3 μs arises from the loss of signal as the field correlation function $g_1(\tau)$ approaches its baseline [Figure 1(a)] and, potentially, additional retardation of tracer diffusion because of the onset of some *p*-NIPAAM cluster formation. No discernable elastic component exists. In the gel phase [Figure 1(c)], the MSD and logarithmic slope α display distinctively more complex behavior. For delay times shorter than approximately 10 μs, the logarithmic slope α starts off near the free diffusion value of 1. Up to delay time of several 100 μs, the slope decreases continuously toward a minimum around 0.15 before slowly recovering to a value near 0.5 at the edge of the delay time range. These data establish that passive microrheology does indeed display the expected switch from diffusive to

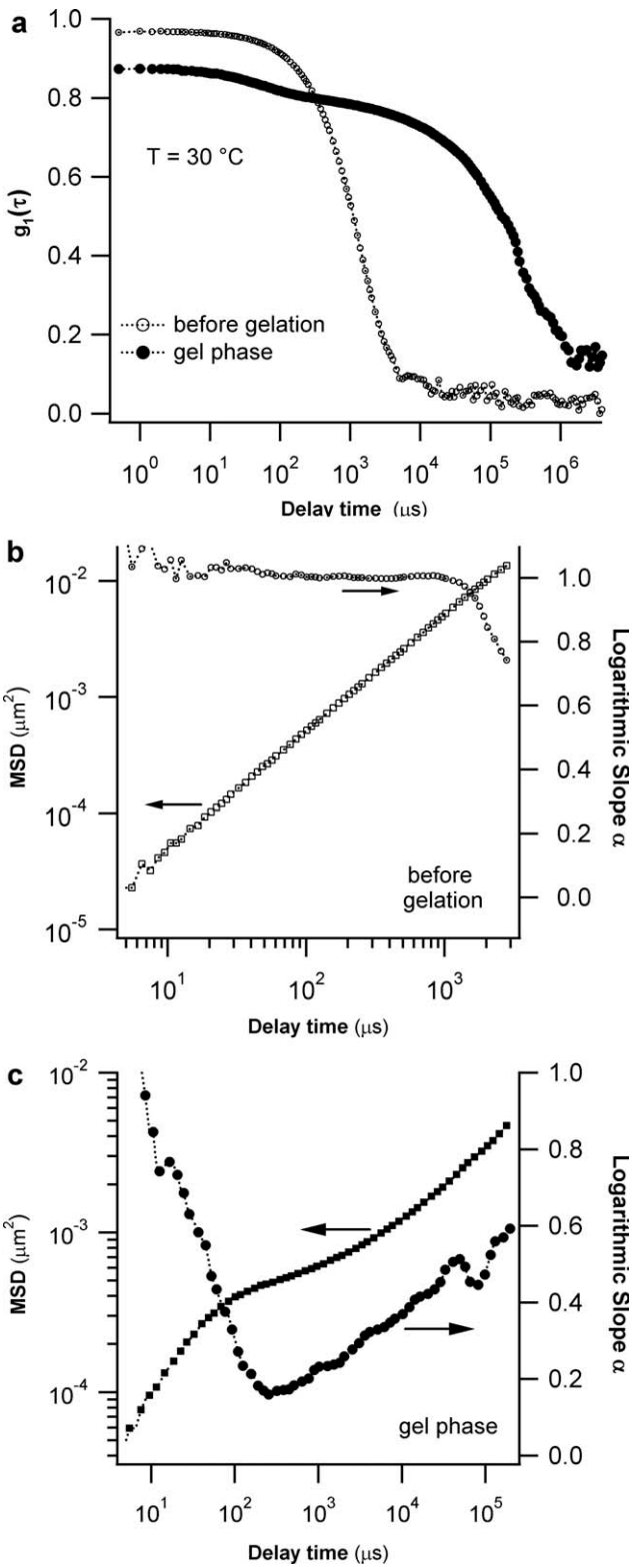

Figure 1. Optical microrheology of sol vs. gel phase of *p*-NIPAAM. (a) Field correlation functions $g_1(\tau)$ for polystyrene beads ($d = 453$ nm) moving in a 5 wt % *p*-NIPAAM well before (○) or after (●) gel formation at 30°C. (b) Log-log plot of the MSD (□) and the corresponding logarithmic slope α (○) vs. delay time τ for bead displacements in the solution before gelation. (c) MSD (■) and logarithmic slope α (●) vs. delay time τ for the corresponding gel phase measurements.

subdiffusive behavior on the transition from a purely viscous solution to a gel phase that spans the entire sample volume. Notice also that, even near the outer edge of our analysis range of 0.2 s [Figure 1(c)], the average displacement of the tracer beads has only reach about $\sqrt{7 \times 10^{-3}\mu m^2} = 83$ nm. This represents a fraction of the 450 nm bead diameter, indicating that the tracer beads only probe linear viscoelastic responses.

Another assumption underlying microrheology with DLS is that the gel is locally homogeneous from the scale of the individual tracer beads up to the size of the detection volume over which the bead motion is averaged (i.e., 0.5–200 μm). To ascertain whether the specific *p*-NIPAAM gels prepared for our measurements fulfill this requirement, we imaged 10 μm thick *p*-NIPAAM strips with beads embedded inside of them. As shown in Figure 2(a), bright field images indicate no optical heterogeneities on these length scales other than those arising from fluorescent bead embedded into the gel. Confocal images of the fluorescent beads embedded within the strips showed that bead motion was tightly coupled to gel motion during thermal contraction, implicating that there are no large voids or other heterogeneities on these length scales. A quantitative analysis of the mean displacement of the beads in the swollen and collapsed state [Figure 2(b)] confirmed the correlated movement of all embedded beads.

High-Frequency Viscoelasticity of *p*-NIPAAM Gels Far Below the Deswelling Transition

For the subsequent experiments, we used gel samples for which the gelation process was complete. Applying the generalized Stokes-Einstein relation or GSER (see Experimental section above), we analyzed the bead motion and derived the elastic and viscous shear moduli G' and G''.[9,15,17] This approach implicitly assumes that the frequencies of bead motion are higher than the coupling frequency f_{long} for which longitudinal compression modes of the gel become overdamped and can be neglected. These longitudinal modes would couple to bead motion and move them around independent of their thermal motion.[9,18] The frequency f_{long} for the onset of overdamping can be estimated as[9]

$$f_{long} \cong (G/\eta_s)(\xi/a)^2 \tag{9}$$

where G is the elasticity of the gel network, η_s, the solvent viscosity, ξ, the gel mesh size, and a, the tracer particle radius. For our system, $G \cong 1$ Pa, $\eta \cong 10^{-3}$ Pa s, $\xi \leq 20$ nm, and $a = 225$ nm, which yields an estimate for the coupling frequency f_{long} of 8 Hz. The mesh size ξ was estimated by the approach outlined by Canal and Peppas.[19] The upper limit of the mesh size is the fully extended length of subchains between crosslinks. As the crosslink density is 2 wt %, the average number of segments in a subchain is 70. The size of a segment is two C—C bonds, or 0.308 nm, and hence the largest possible mesh size is of the order of 20 nm. Hence, the GSER analysis will be applicable over nearly the entire frequency range, with the possible exceptions of the low-frequencies edge probed in our experiments.

Figure 3(a) displays the frequency-dependence of the elastic and viscous moduli G' and G'' at 15°C derived from data such as

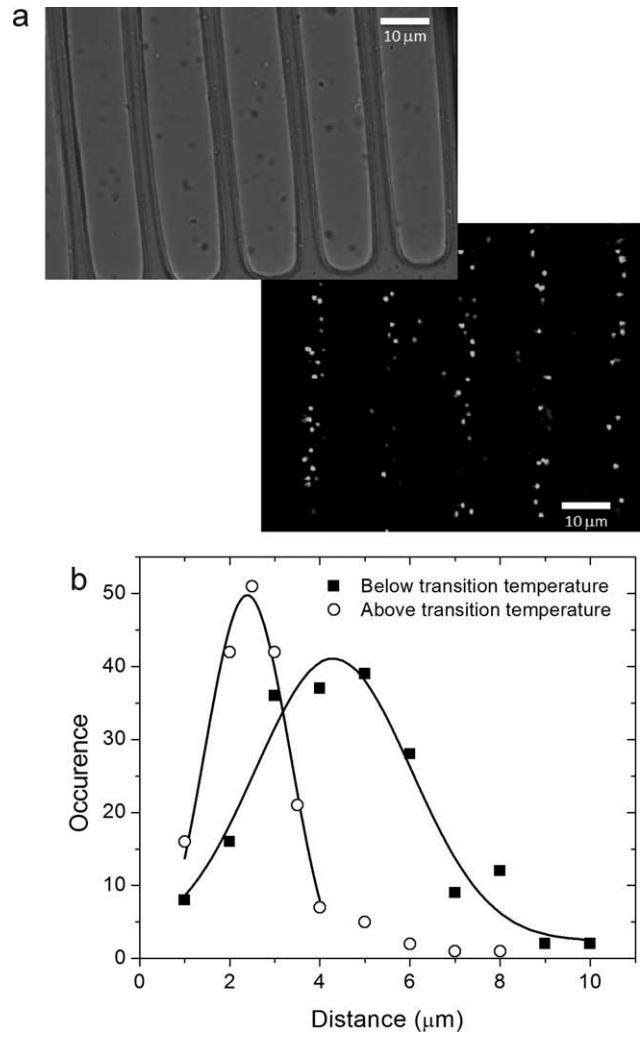

Figure 2. Frequency dependence of elastic and viscous modulus for *p*-NIPAAM gel. (a) Optical micrographs of *p*-NIPAAM gel strips (10 μm dry width by 10 μm dry height) with embedded 500 nm fluorescent polystyrene microspheres. The upper image is a bright field image of a series of gel strips with the embedded beads showing up as dark spots. The lower image shows the same microspheres within a single focal plane of the gel strips after their contraction past the deswelling transition. (b) Plot of the corresponding distribution in relative distances between nearest neighbor microspheres for both states (for details, see Ref. 16).

those in Figure 1 using the GSER analysis [eqs. (4) and (5) in Experimental section]. The magnitude of the elastic modulus ranges from fractions of a Pascal to few tens of a Pascal. This range is typical for soft gels and makes it well suited for passive microrheological measurements. The data span a frequency range of nearly five decades (5–100 kHz). Over this wide frequency range, the elastic modulus increases by approx. one to two orders of magnitude, indicating modest shear stiffening of the gels. Our observations of shear stiffening with increasing frequency match observations in other chemically crosslinked gels including polyacrylamide gels[10], and in biological gels.[9] Over the same frequency range, the logarithmic slope of the elastic modulus decreases continuously from around 0.6 at low frequencies down to 0.15 at frequencies at or above 10 kHz. Because frequency- and length scales are directly correlated via the MSD of the probe particle, the increase in G' with increasing frequency is consistent with stiffening of the *p*-NiPAAM gels at shorter length scales. The observed stiffening likely results from the numerous degrees of network relaxation that become frozen out when the motion of the polymer gel is constrained to very short displacements (<10 nm).

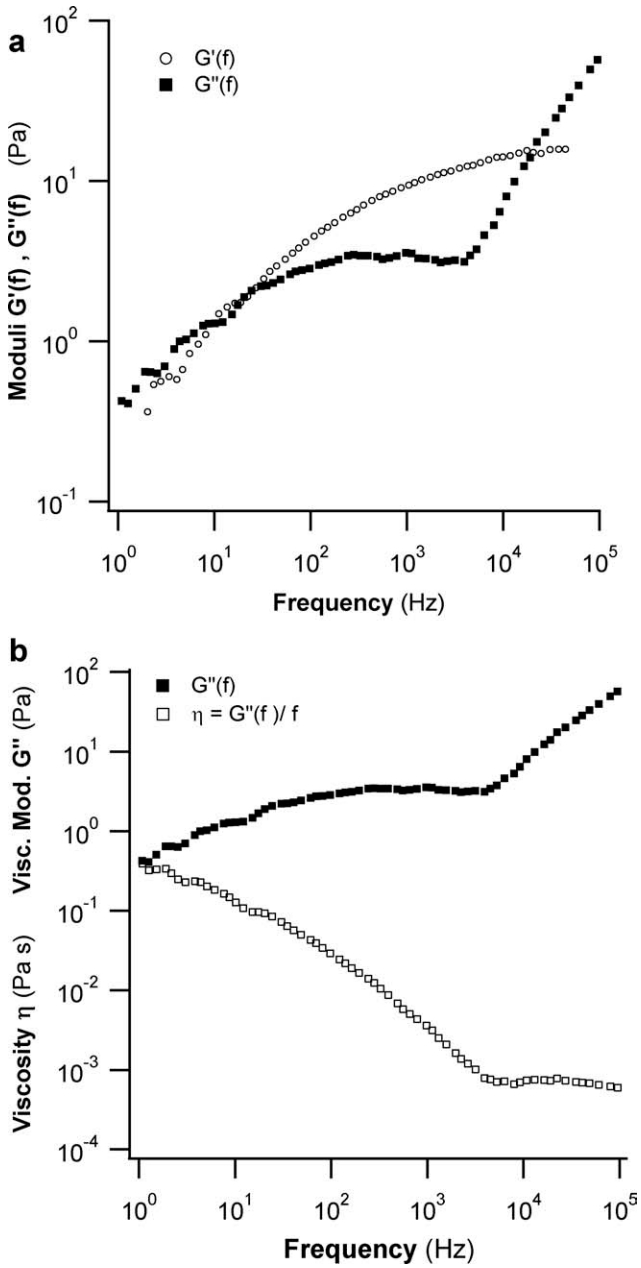

Figure 3. Frequency dependence of elastic and viscous modulus for *p*-NIPAAM gel. (a) Elastic modulus G' (○) and viscous modulus G'' (■) for *p*-NIPAAM gel as function of probe frequency for a fixed temperature of 15°C. (b) Viscous modulus G'' (■) together with the derived viscosity $\eta = G''/f$ (□). Initially, gel viscosity η drops off with increasing frequency. On reaching a crossover frequency f_{cross} of approx. 5 kHz, viscosity plateaus off close to the solvent viscosity η_s.

Figure 3(a,b) also display the frequency-dependent viscous dampening of the bead motion in the gel/solvent matrix. The viscous modulus G'' initially increases slightly, with its logarithmic slope decreasing from about 0.5 near 10 Hz to almost 0 when approaching 5 kHz. It then abruptly increases beyond $f_{cross} = 5$ kHz, with a logarithmic slope constant and close to 1. The corresponding viscosity $\eta = G''(f)/f$ [Figure 3(b)] provides a more intuitive explanation for the observed transition in the frequency dependence for the loss modulus G''. Below the crossover frequency, viscous loss steadily increases as frequency decreases. This correlates well with the progressive loss of gel elasticity with decreasing frequency. The high-frequency increase in the viscous modulus near 5 kHz, in turn, corresponds to a plateau in the viscosity that is close to water viscosity η_w at that temperature. To test whether this transition is indeed indicative of an intrinsic change in the temporal dynamics of *p*-NIPAAM gels and not because of an intrinsic length scale set by the probe particles or the gel, we repeated the measurements with 200 nm and 900 nm beads. No change in crossover frequency was observed. The persistent increase in gel elastic modulus beyond the crossover frequency of the viscous modulus further indicates that the transition in viscous dissipation is not due to, for example, probe beads being trapped in a small solvent cage.

These observations suggest that above f_{cross} viscous losses are controlled by dissipation within the solvent phase; below the crossover frequency, in contrast, losses from dissipation within the gel dominate. Theoretically, this crossover is expected to occur for frequencies at which the viscous and elastic moduli of the gel are smaller than the viscous shear stress in the solvent.[20] The solvent shear stress modulus can be estimated as the product of solvent viscosity η_s and probe frequency f. Using the viscosity of water (10^{-3} Pa s) for solvent viscosity, the solvent shear stress modulus will therefore become comparable with the elastic modulus of the gel matrix ($\sim$ 1–10 Pa) for frequencies of a few kHz (1–10 kHz). This simplified estimate for the crossover frequency f_{cross} matches well with our experimentally observed values. Such crossover in gel dissipation has been observed experimentally in soft colloidal gels.[21] In many gel systems reported in literature, however, shear stiffening of the gel with frequency is much more pronounced than for the soft *p*-NIPAAM gels in our experiments. As a result f_{cross} is located beyond the high-frequency limits of microrheology even when using diffusing wave spectroscopy. To our knowledge, the *p*-NIPAAM data here represent the first time such frequency-dependent crossover from gel to solvent-dominated loss modulus has been observed in a chemically crosslinked polymeric network.

Overall, our high-frequency rheological data do not reach the low-frequency plateau values for G' and G'' characteristic of crosslinked gels.[10,22] However, particularly for the soft gel we investigated, plateau values are only expected below the low-frequency limit f_{long} imposed on the GSER analysis [see eq. (9) above]. It is worth noting that the log-log plots for the elastic modulus G' and, below f_{cross}, the loss modulus G'' lack a power-law scaling regime with probe frequency. Such power-law scaling has been observed experimentally and predicted theoretically for frequencies beyond the low-frequency elastic plateau.[9,23] Power-law scaling also accounts for the much steeper increase in gel elasticity with frequency observed with microrheology in these other systems. We hypothesize that the structure of the *p*-NIPAAM gels varies across different length scales, thereby eliminating the characteristic length scale underlying frequency-dependent scaling-laws.

Viscoelasticity of *p*-NIPAAM Gel on Approach Toward the Deswelling Transition

The above measurements explored the generic behavior of *p*-NIPAAM gel viscosity and elasticity at high frequencies. The subsequent experiments were focused on temperature-induced changes in the viscoelastic response on approach to the deswelling transition. As discussed below, changes in intrinsic light scattering intensity with gel temperature follow a power law, thereby indicating that the deswelling transition under our conditions is of second order. Because intrinsic scattering intensity is directly related to bulk compressibility, the gel bulk modulus is bound to displays the power-law behavior typical for second order transitions. Near the critical point, theoretical considerations predict pronounced modulation in the bulk modulus, but only a step-change in the shear modulus past the transition and no discernable modulation on approach to the transition temperature.[24] We were interested whether, at our off-critical concentrations, the shear modulus of *p*-NIPAAM obtained from the microrheological measurements also developed temperature-dependent power-law behavior, remained constant, or showed distinct temperature dependencies in different frequency regions. Figure 4(a) displays the frequency-dependence of the elastic modulus G' for a series of temperatures approaching the deswelling temperature, which for our gels occurs at $T_{cp} = 33°C$. The overall frequency dependence of G' is similar at all temperatures, with gel elasticity undergoing comparable shear thickening as frequency increases. For any fixed frequency, however, the magnitude of the elastic modulus G' decreases on approach towards T_{cp}. This becomes apparent when plotting G' vs. the reduced temperature $\varepsilon = (T_{cp} - T)/T_{cp}$ for a series of different frequencies [Figure 4(b)]. The solid lines in Figure 4(b) represent power law fits of the form $G' \% \varepsilon^{v}$ near the cloud point temperature T_{cp}. These fits indicate that the temperature dependence of the elastic modulus displays power-law behavior, with an exponent that is independent of probe frequency. However, as indicated by our intrinsic light scattering data below, these gel samples are not near the critical point in the phase diagram.[25] Hence, comparison with critical scaling exponents is not meaningful. The power law exponents quoted here are therefore used solely as a means of quantifying the observed temperature dependence of G' and G'' (see below) on approach toward the deswelling transition.

Figure 5(a) presents the temperature-induced changes to the viscous modulus G'' and corresponding gel viscosity η. In contrast to the elastic modulus, the temperature dependence for viscous dissipation is clearly distinct for frequencies below and above the crossover frequency f_{cross}. As discussed above, dissipation below f_{cross} is dominated by dissipation within the gel matrix whereas solvent-mediated dissipation dominates above f_{cross}. Hence, we plotted the viscosity η against the reduced temperature ε only for frequencies $f < f_{cross}$, which quantify gel

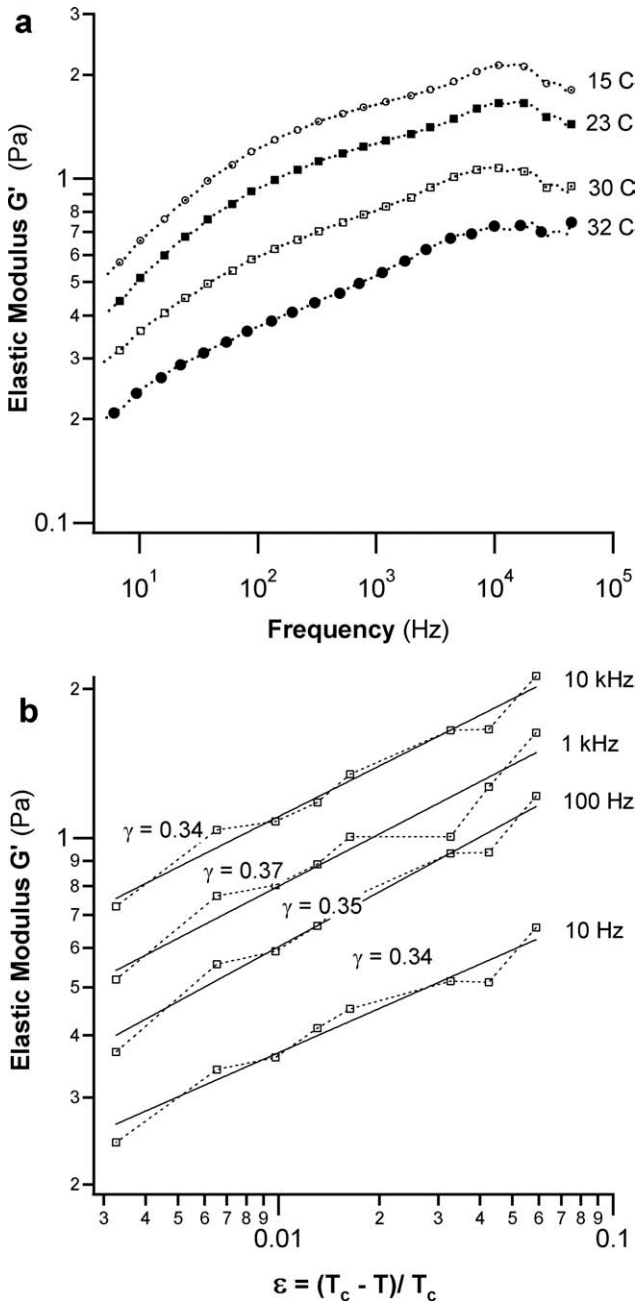

Figure 4. Temperature-dependence of elastic modulus G'. (a) Elastic modulus G' *vs.* frequency for p-NIPAAM gel as temperature approaches the gel collapse temperature of $T_{cp} = 33$ °C. (b) Temperature-dependence of the elastic modulus G' vs. reduced temperature $\varepsilon = (T_{cp} - T)/T_{cp}$ at four different frequencies. Solid lines represent power-law fits through the data of the form $G' \% \varepsilon^{\gamma}$.

dissipation [Figure 5(b)]. In this regime, gel viscosity displays temperature dependence similar to the elastic modulus. The solid lines in Figure 5(b) again represent power-law fits through the data points. Beyond the crossover frequency, the viscous modulus only reproduces the comparatively weak temperature-dependence of solvent viscosity.

The power-law exponents for the viscous and elastic moduli were independent of probe frequency but were clearly distinct from one another. Within a given gel, the absolute values for the elastic and viscous coefficients varied with measurement locations, but their corresponding thermal power-law coefficients were similar. However, the power-law exponents obtained from different samples varied significantly. For example, the power law coefficients for the viscosity of three different samples were 0.23 ± 0.05; 0.43 ± 0.03; and 0.51 ± 0.05, respectively. Given that the exponents obtained from the same gel were reproducible, we presume that these variations reflect

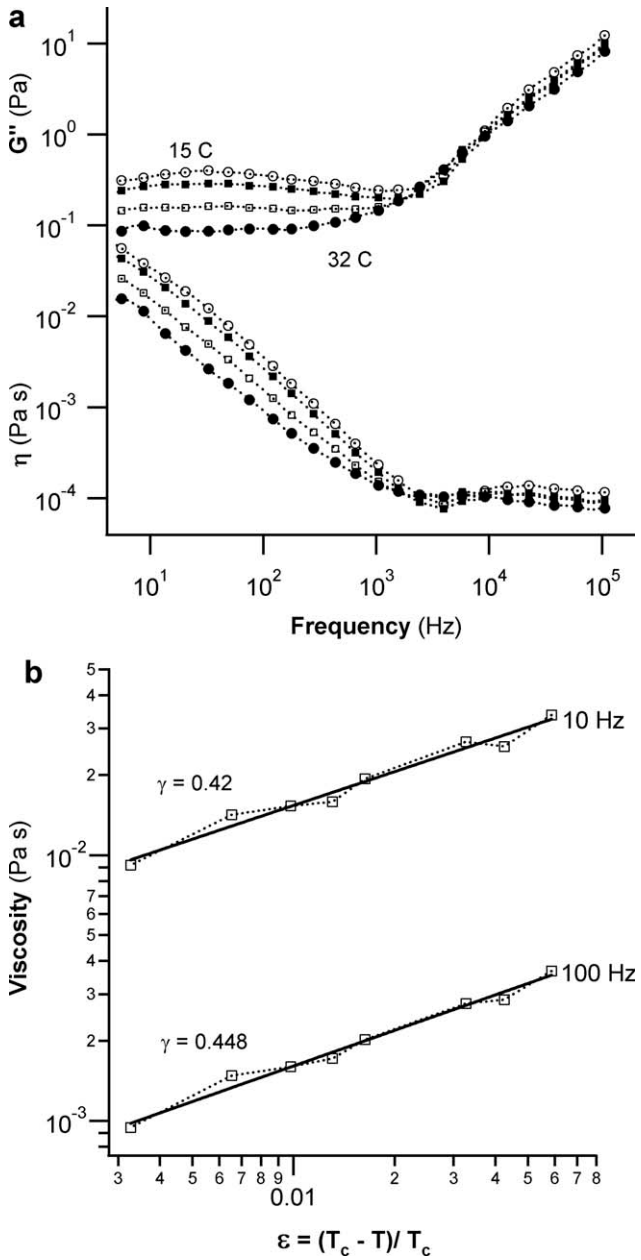

Figure 5. Temperature dependence of viscous modulus G'' and viscosity η. (a) Viscous modulus G'' and viscosity η vs. frequency for *p*-NIPAAM gel on approach toward the gel collapse temperature of $T_{cp} = 33$°C. (b) Viscosity $\eta = G''/f$ at two fixed frequencies below f_{cross} vs. reduced temperature $\varepsilon = (T_{cp} - T)/T_{cp}$. Solid lines are power law fits of the form $\eta \% \varepsilon^{\gamma}$.

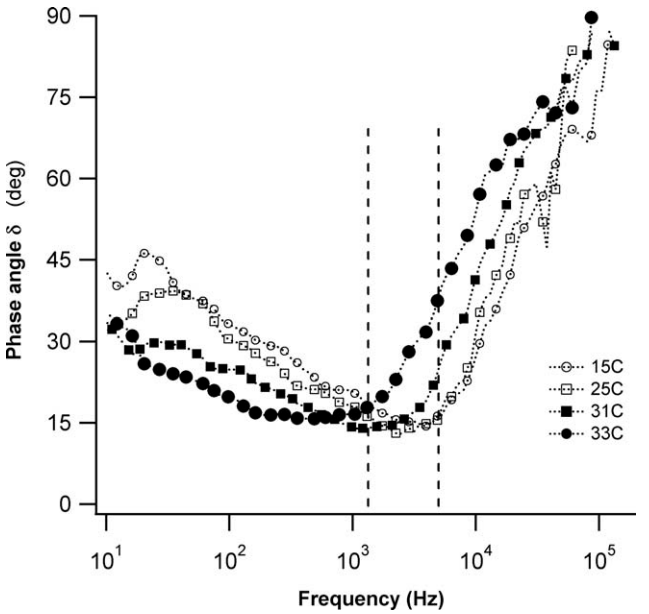

Figure 6. Phase angle of viscoelastic moduli for *p*-NIPAAM gels. Phase angle $\delta = \arctan(G''/G')$ for the elastic and viscous moduli as function of frequency f and at the four indicated temperatures. The vertical, dashed lines indicate the frequency range for the temperature-induced shift in the crossover frequency f_{cross}.

global variations in overall crosslink density and gel structure that are beyond the control of our sample preparation protocol. Such differences are bound to affect the off-critical pathway a specific gel follows in approaching the deswelling transition (Figure 7). Given that the power-law coefficients along these off-critical pathways are distinct from universal scaling coefficients in the first place, it seems plausible that these differences reflect the differences among distinct off-critical pathways.

Figure 6 displays the phase angle $\delta = \arctan(G''/G')$ for the data in Figures 3 and 4. This phase plot highlights the relative

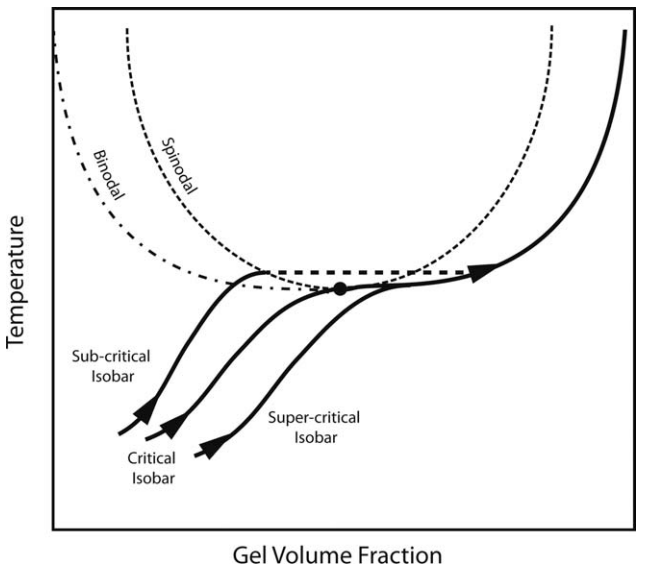

Figure 7. Phase separation and *p*-NIPAAM phase diagram. Schematic of the *p*-NIPAAM phase diagram (with binodal and spinodal phase boundary) and three distinct pathways towards phase separation. Gels reaching the binodal curve along a subcritical isobar will undergo a first-order transition and contract discontinuously until reaching the high-concentrations phase along the solid binodal. When following a super-critical isobar, gels will move along the binodal to their new equilibrium volume fraction, making this a second order transition. See also discussion and Ref. in text.

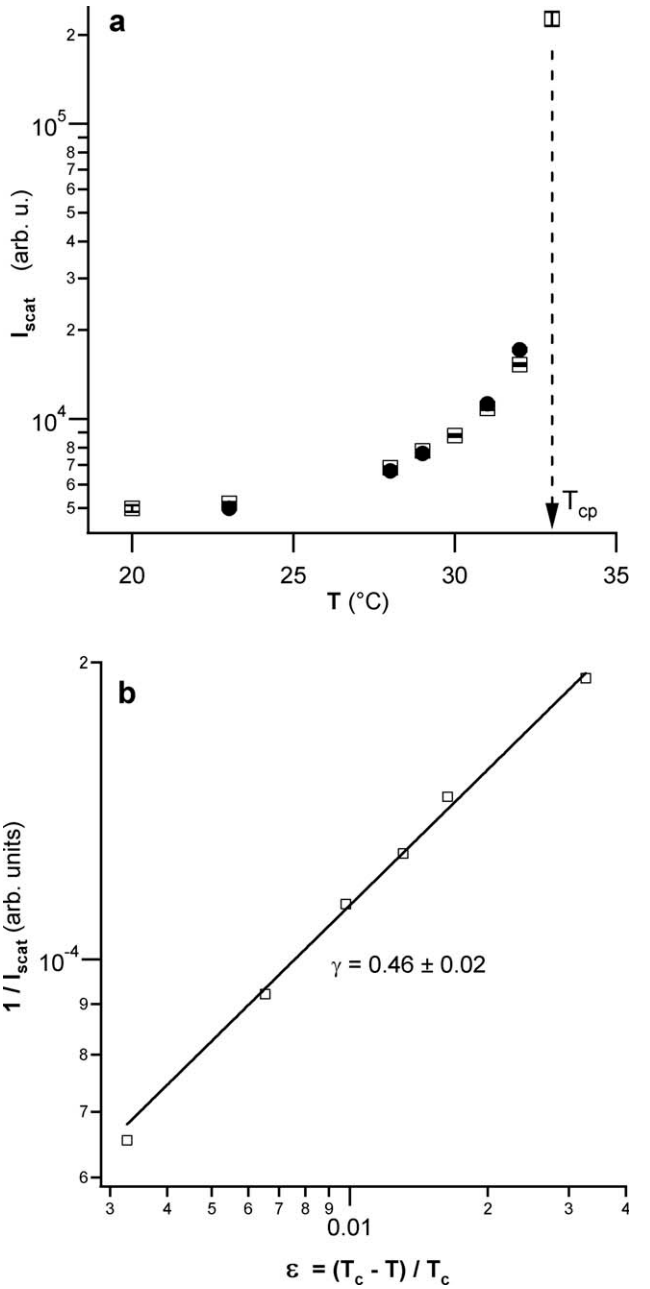

Figure 8. Static light scattering from *p*-NIPAAM gels without beads. (a) Lin-log plot of the intrinsic scattering intensity I_{scat} of *p*-NIPAAM gel vs. temperature on heating toward (□) and cooling down from (■) its collapse temperature of $T_{cp} = 33°C$. Notice the absence of any hysteresis on crossing the transition from different directions. (b) Log-log plot of inverse scattering intensity vs. the reduced temperature $\varepsilon \equiv (T_{cp} - T)/T_{cp}$. The solid line is a power law fit through the data.

importance of elastic vs. viscous modes at different probe frequencies. Several features of this plot are noteworthy. For any fixed temperature and for frequencies beyond the crossover frequency f_{cross}, the phase angle rapidly increases toward 90°. In this regime, solvent dissipation dominates tracer motion over contributions from both viscous and elastic gel moduli. This is consistent with the assumptions underlying the estimate for the crossover frequency in eq. (9). At frequencies below f_{cross}, the phase angle remains below 45°, indicating that the elastic shear modulus dominates over viscous dissipation. Comparing the magnitude of the phase angles δ for fixed frequencies $f < f_{cross}$ but for increasing temperature, it becomes apparent that the elastic contribution becomes more prominent as gel temperature approaches T_{cp}. This temperature-trend becomes reversed at high frequencies. The crossover frequency from gel to solvent-dominated viscosity [e.g., Figure 5(a)] coincides with the location of the minimum in the phase angle plot. The plot also indicates that the crossover frequency itself is a weak function of solvent temperature, shifting toward lower frequencies as the temperature approaches T_{cp}. Again, this is expected based on the dependence of the crossover frequency f_{cross} on G and from the observed softening of the gels when approaching T_{cp}.

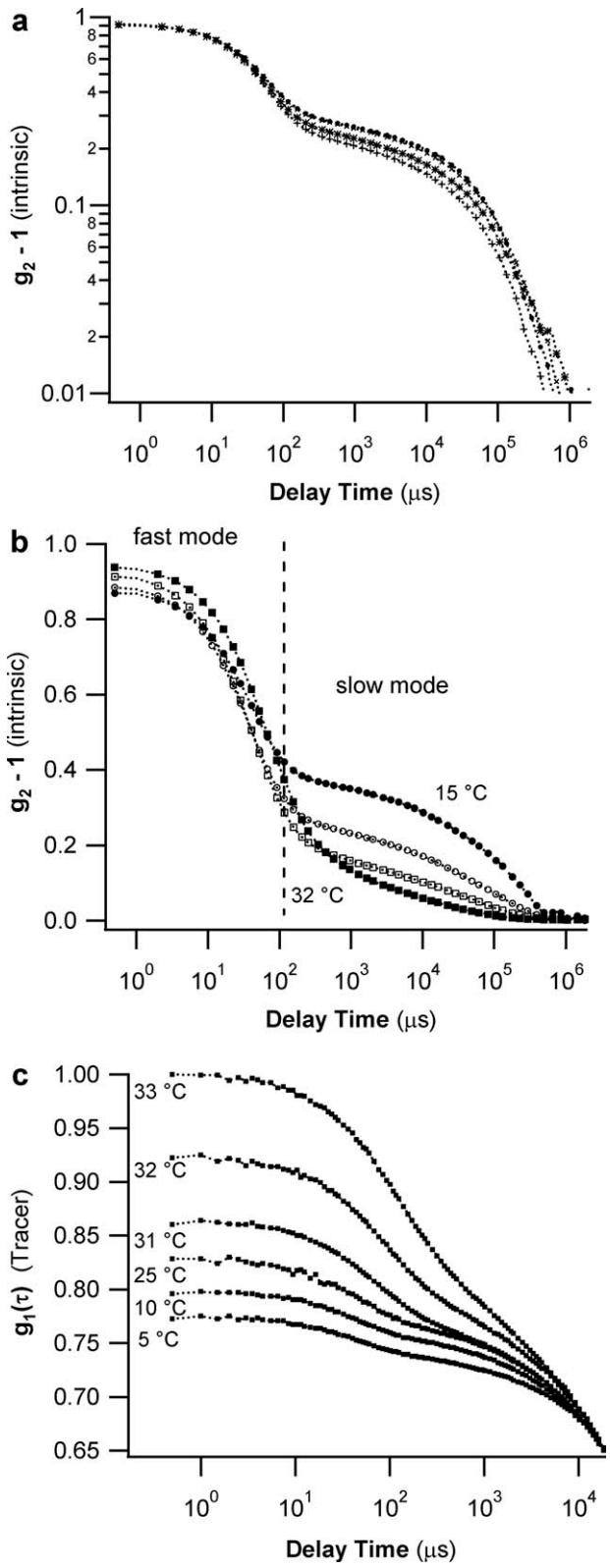

Figure 9. Intrinsic dynamics of *p*-NIPAAM gels probed by DLS. (a) Normalized intensity correlation function, $g_2(t) - 1$, for light scattered from *p*-NIPAAM gels without beads at a fixed temperature (23°C) but four different positions within the same gel sample. (b) Intensity correlation functions for *p*-NIPAAM gel sample without beads measured at a single position but for four different sample temperatures (15°C, 23°C, 28°C, 32°C). Notice the presence of a fast and slow decay mode. (c) Field correlation functions $g_1(\tau)$ obtained during microrheological measurements (*p*-NIPAAM with beads) at different temperatures. Values for different $g_1(\tau)'$s were matched at some (arbitrarily chosen) delay time (~ 20 ms). As the gel temperature approaches its collapse temperature (T_{cp}), the field correlation function at short delay times (0.1–1 ms) displays an increasingly prominent fast decay mode. Notice the close match in the frequency for the intrinsic fast mode of *p*-NIPAAM gels and the fast mode emerging during microrheological measurements.

Intrinsic Light Scattering from *p*-NIPAAM Gels

We used intrinsic light scattering from *p*-NIPAAM gels without tracer beads to address questions raised by the above microrheological measurements. Specifically, we determined whether the deswelling transition, under our experimental conditions, was a second order or first order transition. In addition, we investigated whether the intrinsic dynamics of *p*-NIPAAM gels could be related to the rheological properties obtained from tracer bead motion.

On warming to near physiological temperatures, *p*-NIPAAM gels undergo a dramatic volume transition to a collapsed state. The constraints imposed on the gel by the chemical crosslinks causes the gel to either undergo a first order or second order transition toward the collapsed state (Figure 7). The curved isobars indicate that the gels on an increase in temperature will begin to contract even before reaching the phase separation binodal. Gels reaching the binodal along a subcritical isobar will enter the two-phase region (solid curve between binodal and spinodal) and discontinuously "toward" the high-concentration boundary of the binodal (dashed line). Gels above the critical isobar, in contrast, will "slide" along the binodal to reach their

new equilibrium volume fraction (for details, see Ref. 25). Notice, in addition, that samples away from the critical isobar will pass in close proximity to the critical point and the large concentration fluctuations prevailing there. We did not know *a priori* whether our samples will follow a sub- or supercritical isobar toward the phase separation boundary. The static light scattering measurements we performed were aimed at addressing this question. Intrinsic light scattering from gels prepared following our protocol displayed a deswelling transition at $T = 33°C$ [Figure 8(a)]. The change in scattering intensity on gel collapse occurs at the same temperature, irrespective whether the transition is approached from the low-temperature, swollen phase (open symbols) or high-temperature, collapsed phase [solid symbols in Figure 8(a)]. Furthermore, the scattering intensity I_{scat} increases noticeably well before reaching the transition temperature. The corresponding drop off in $1/I_{scat}$ vs. the reduced temperature $\varepsilon = (T_{cp} - T)/T_{cp}$ follows the power-law behavior typical for critical fluctuations. The lack of hysteresis in the scattering intensity on crossing the transition temperature and the presence of critical fluctuations below the transition indicate that *p*-NIPAAM sample conditions are sufficiently close to the critical point to render the transition essentially second-order in nature. The power-law coefficient of $\gamma = 0.46$ for the scattering intensity [Figure 8(b)], however, is clearly distinct from the experimentally determined critical coefficient of 1.0[26] or theoretically predicted value of 1.2.[3] Hence, as pointed out above, the gel samples do appear to follow a super-critical isobar and to pass close enough to the critical point to pick up large fluctuations and undergo a second order phase transition. The power law fits and coefficients derived in this work, therefore, only provide a way to quantify the overall behavior for these gel samples on their approach toward their off-critical deswelling transition.

We used DLS to investigate whether and to what extent several features in the microrheology of *p*-NIPAAM gel relate to the intrinsic dynamics of *p*-NIPAAM gels seen with DLS in the absence of tracer particles. We measured the intrinsic correlation functions of *p*-NIPAAM gels at a fixed temperature but at different locations within the same sample [Figure 9(a)]. Overall, the intensity correlation functions show a bimodal decay observed for a variety of gel systems. Although the decay rates of both the fast and slow mode are very similar, their relative amplitudes vary slightly with measurement location. Such minor heterogeneities in the intrinsic dynamics are expected.[27] Although we couldn't map out the dependence on the scattering vector q for either mode with our DLS system, the observed crossover from slow to fast modes matches well with other observations of bimodal decay in crosslinked gels.[28,29]

We also investigated the temperature-induced changes in the intrinsic dynamics of *p*-NIPAAM gels [Figure 9(b)]. With increasing temperature, the fast relaxation mode of the gels becomes slightly more prominent whereas the slow mode decreases significantly. Several aspects of these intrinsic dynamics correlate closely to features in the *p*-NIPAAM microrheological measurements. Most noticeably, the transition from fast to slow mode decay in the intrinsic dynamics occurs very close to the crossover from gel- to solvent-dominated viscous dissipation. This is consistent with the interpretation of the fast mode as "gel modes" for which the gel network moves relative to the solvent background. As a result, viscous dissipation of embedded tracers becomes dominated by motion of the beads against the solvent background, as seen in the microrheological measurements. Similarly, the softening of the gel elastic modulus and increase in its viscous modulus on approach to the deswelling temperature are reflected in the decline of the amplitude of the slow modes seen in intrinsic correlation data [Figure 9(b)].

The correlation functions of the tracer particles themselves contain a direct signature of the transition from gel- to solvent-dominated viscosity. Figure 9(c) shows an overlay of the field correlation functions $g_1(\tau)$ obtained with tracer beads over a limited range of delay times, corresponding to frequencies at or above the crossover frequency f_{cross}. The values for the $g_1(\tau)'$s at different temperatures were arbitrarily matched to a point near 20 ms delay time. This overlay highlights the presence of both a fast and a slow decay mode in the microrheology correlation functions for the tracer beads. The fast decay mode at short delay times becomes significantly more prominent as the temperature approaches the cloud point temperature. With increasing temperature the gel softens, making it easier to excite gel modes and leading to an increasing dominance of solvent viscosity over both gel elasticity and viscosity. As a result, the contributions of solvent dissipation to thermal bead motion become increasingly more prominent even in the raw correlation data.

CONCLUSIONS

High-frequency optical microrheology reveals several basic features of the viscoelastic behavior of *p*-NIPAAM gels not readily accessible with either bulk rheometers or videomicroscopy-based microrheology.[30] First, the data uncover the crossover from gel- to solution-dominated viscous dissipation at frequencies around 5 kHz. The match with theoretical predictions and with intrinsic "gel modes" in the sample indicate that this crossover is related to the onset of relative motion of the network against the solvent background. Second, the elastic modulus of *p*-NIPAAM gels displays modest shear thickening, consistent with enhanced gel elasticity at short length- or time scales. At the same time, *p*-NIPAAM elasticity decreases as solution temperature increases toward the deswelling transition. This behavior is in contrast to the entropy-driven increase in elasticity typical for rubber (see e.g., Ref. 31) but is consistent with the intuitive idea that changes in polymer interactions, and not entropic contributions, drive free energy changes during the approach toward the collapse temperature T_{cp}. Finally, both the viscosity and elastic modulus of *p*-NIPAAM gels decrease near the cloud point temperature following power-laws reminiscent of critical behavior near a critical point. Although seemingly independent of frequency, the power-law exponents do vary from sample to sample. These variations are likely indicative of differences in gel structure induced during the gelation process, which are clearly more prominent than the weak modulation in intrinsic gel dynamics observed at different locations within the same sample.

ACKNOWLEDGMENTS

This research was supported, in part, through the University of South Florida Research and Education Initiative under Grant

GFMMD02 (R. T. & M. M.), an NSF CAREER award DMR-0645574 (R. T.), FMMD summer support (M. M.), and an NSF IGERT fellowship (S. H.). We also would like to acknowledge the helpful discussions with David Weitz during early stages of this work.

REFERENCES

1. Li, Y.; Tanaka, T. *Annu Rev. Mater. Sci.* **1992,** *22*, 243.
2. Hirokawa, Y.; Tanaka, T. *J. Chem. Phys.* **1984,** *81*, 6379.
3. Shibayama, M.; Tanaka, T. *Adv. Polym. Sci.* **1993,** *109*, 1.
4. DuPont, S. J.; Cates, R. S.; Stroot, P. G.; Toomey, R. *Soft Matter* **2010,** *6*, 3876.
5. Hirotsu, S. *J. Chem. Phys.* **1991,** *94*, 3949.
6. Hirotsu, S. *Macromolecules* **1990,** *23*, 903.
7. Shibayama, M.; Morimoto, M.; Nomura, S. *Macromolecules* **1994,** *27*, 5060.
8. Mason, T. G.; Ganesan, K.; van Zanten, J. H.; Wirtz, D.; Kuo, S. C. *Phys. Rev. Lett.* **1997,** *79*, 3282.
9. Schnurr, B.; Gittes, F.; MacKintosh, F. C.; Schmidt, C. F. *Macromolecules* **1997,** *30*, 7781.
10. Dasgupta, B.; Weitz, D. A. *Phys. Rev. E* **2005,** *71*, 021504.
11. Scheffold, F. Schurtenberger, P. *Soft Materials*, **2003**, *1*, 139.
12. Gardel, M. L.; Valentine, M. T.; Weitz, D. A. In Microscale Diagnostic Techniques; Breuer, K., Ed.; Springer-Verlag: New York, **2005.**
13. Chen, D. T.; Weeks, E. R.; Crocker, J. C.; Islam, M. F.; Verma, R.; Gruber, J.; Levine, A. J.; Lubensky, T. C.; Yodh, A. G. *Phys. Rev. Lett.* **2003,** *90*, 108301.
14. Jakeman, E. In Photon Correlation and Light Beating Spectroscopy, Cummins, H. Z., Pike, E. R., Eds.; Plenum Press: New York, **1974;** p 75.
15. Mason, T. G. *Rheol. Acta* **2000,** *39*, 371.
16. Bello, C. A. Microsphere-aided characterization of stimuli-responsive polymeric networks, M. Eng. Thesis., University of South Florida: Tampa, **2008;** p 89.
17. Mason, T. G.; Weitz, D. A. *Phys. Rev. Lett.* **1995,** *74*, 1250.
18. Levine, A. J.; Lubensky, T. C. *Phys. Rev. Lett.* **2000,** *85*, 1774.
19. Canal, T.; Peppas, N. A. J. *Biomed. Mater. Res.* **1989,** *23*, 1183.
20. Levine, A. J.; Lubensky, T. C. *Phys. Rev. E* **2001,** *63*, 041510.
21. Prasad, V.; Trappe, V.; Dinsmore, A. D.; Segre, P. N.; Cipelletti, L.; Weitz, D. A. *Faraday Discuss* **2003,** *123*, 1.
22. Gil, E. S.; Hudson, S. M. *Biomacromolecules* **2007,** *8*, 258.
23. Doi, M.; Edwards, S. F. The Theory of Polymer Dynamics;Oxford University Press: New York, **1987.**
24. Hirotsu, S. *Phase Transit* **1994,** *47*, 183.
25. Vidyasagar, A.; Smith, H. L., Majewski, J., Toomey, R. G. *Soft Matter* **2009,** *5*, 4733.
26. Tanaka, T.; Ishiwata, S. I.; Ishimoto, C. *Phys. Rev. Lett.* **1977,** *38*, 771.
27. Xue, J. Z.; Pine, D. J.; Milner, S. T.; Wu, X. l.; Chaikin, P. M. *Phys. Rev. A* **1992,** *46*, 6550.
28. Gianneli, M.; Roskamp, R. F.; Jonas, U.; Loppinet, B.; Fytas, G.; Knoll, W. *Soft Matter* **2008,** *4*, 1443.
29. Tanaka, Y.; Gong, J. P.; Osada, Y. *Prog. Polym. Sci.* **2005,** *30*, 1.
30. Cicuta, P.; Donald, A. M. *Soft Matter* **2007,** *3*, 1449.
31. Rubinstein, M.; Colby, R. H. Polymer Physics; Oxford University Press: Oxford, **2003.**